Tellus (1980) *32*, 348–364

Linear theory of stratified hydrostatic flow past an isolated mountain

By RONALD B. SMITH, *Department of Geology and Geophysics, Yale University, 2161 Yale Station, New Haven, CT 06520, U.S.A.*

(Manuscript received August 22; in final form December 28, 1979)

ABSTRACT

The stratified hydrostatic flow over a bell-shaped isolated mountain is examined using linear theory. Solutions for various parts of the flow field are obtained using analytical and numerical Fourier analysis. The flow aloft is composed of vertically propagating mountain waves. The maximum amplitude of these waves occurs directly over the mountain but there is also considerable wave energy trailing downstream along the parabolas

$$y^2 = \frac{Nzax}{U}$$

Near the ground, the asymmetric pressure field causes the incoming streamlines to split to avoid the mountain and this lateral deflection persists downstream. The horizontal divergence associated with this lateral deflection is balanced by the descent of potentially warmer air from aloft. The relationship of linear theory to other three-dimensional models is discussed. The approach to the two-dimensional infinite ridge limit and non-hydrostatic effects are also discussed.

1. Introduction

The perturbation to a stably stratified airstream by uneven terrain has been examined theoretically by a number of authors, but only a few have avoided the two-dimensional infinite-ridge assumption and considered the flow past an isolated mountain. Wurtele (1957), and later Crapper (1959, 1962), extended the linear theory of Lyra and Queney, with uniform incoming U and N, to three dimensions but succeeded in describing only the far-field inherently non-hydrostatic "dispersive tail" of the mountain wave disturbance. In a similar way, the work of Scorer and Wilkinson (1956), Palm (1958), Sawyer (1962), Crapper (1962) and Gjevik and Marthinsen (1977) have extended the study of the inherently non-hydrostatic trapped lee waves in structured atmospheres to three dimensions. The nature of the hydrostatic part of the mountain wave disturbance (i.e. those features that remain, under circumstances when the hydrostatic assumption is valid) and the nature of the flow near the mountain, remain largely unknown. It is the intention of this paper to reexamine the small-amplitude theory to clarify these points.

Scorer (1956) attempted to solve a similar problem using an approximate inverse method—the accuracy of which is difficult to estimate. More fundamentally, however, Scorer used an incorrect radiation condition aloft and thus his flow field is composed of downward propagating waves coming from a supposed source, high in the atmosphere. Still, at certain levels, Scorer's patterns of vertical displacement resemble those to be presented here—with the signs reversed.

Blumen and McGregor (1976) used a numerical eigenfunction technique to find the hydrostatic wave field above an isolated mountain with nearly circular contours in both laterally sheared and unsheared flow. Their computation of the wave field in the unsheared case is qualitatively similar to the results to be presented herein.

We shall see that the small-amplitude theory describes the tendency of the flow to be diverted around the mountain but that this theory is valid only for large Froude number $F \equiv U/hH \gg 1$. In the opposite limit, $F \equiv U/hN \ll 1$, the slow incoming flow (U), strong stratification (N) and great mountain height (h), demand that the flow pass around the mountain with fluid particles

0040-2826/80/040348-17$02.50/0

remaining nearly in horizontal planes. Drazin (1961) has shown how the weak vertical pressure gradients which arise in such a flow, can be balanced hydrostatically by generating slight vertical motions. Unfortunately, even though the *small* Froude number theory can predict vertical motions, and the *large* Froude number theory can predict the horizontal deflection of flow to avoid the mountain, the two theories remain distinct and unconnectable, although qualitatively complementary.

The formulation used herein is essentially that of Wurtele (1957) where the horizontal structure of the mountain and the disturbance are represented as a two-dimensional Fourier Transform and the vertical structure is simplified by assuming that the incoming wind (U) and buoyancy frequency (N) are constant with height. The difficulty in evaluating the inverse Fourier Transform is overcome in two ways: (1) The flow over a mountain of arbitrary shape, with or without the hydrostatic assumption, is obtained by numerical analysis using a two-dimensional Fast Fourier Transform (FFT) algorithm. These numerical solutions by themselves however, provide only limited insight into the dynamics. (2) By choosing a mountain of simple shape, and making the hydrostatic assumption, analytical solutions may be obtained for the flow near the ground and in the wave field which trails aloft. These analytical solutions are more useful for clarifying the underlying dynamics.

In Section 2 the mathematical model is described and the numerical results are presented. Section 3 considers the three-dimensional pattern of mountain waves aloft using both asymptotic methods and group velocity arguments. In Section 4 the flow near the ground is described using analytical solutions for the pressure, velocity, and displacement fields. The criterion for the validity of linear theory and the conditions which lead to flow around the mountain, are discussed in Section 5. In Section 6, the approach towards two dimensionality is examined by considering the flow near the end of a long ridge. The changes associated with deviations from hydrostatic balance are discussed in Section 7.

2. The mathematical model

Consider the steady flow of a vertically unbounded, stratified Boussinesq fluid, over small-amplitude topography described by $z = h(x,y)$. The perturbations to the background wind, pressure, and density fields are described by the linearized equations

$$\rho_o U u'_x = -p'_x \tag{1a}$$

$$\rho_o U v'_x = -p'_y \tag{1b}$$

$$\rho_0 U w'_x = -p'_z - \rho' g \tag{1c}$$

$$u'_x + v'_y + w'_z = 0 \tag{1d}$$

$$\rho' = -\frac{d\bar{\rho}}{dz}\eta \tag{1e}$$

where x, y, z are the downstream, cross stream and vertical coordinates; u', v', w', ρ', p', η are the corresponding perturbation velocity components and the perturbation density, pressure and vertical displacement; and ρ_0, U, $d\bar{\rho}/dz$ are the background mean density, wind speed, and vertical density gradient. Using the kinematic condition for steady flow

$$w' = U\eta_x \tag{2}$$

and with U taken as a constant, system 1 can be reduced to a single equation for $\eta(x,y,z)$ the vertical displacement of a fluid parcel, or a density surface, above its undisturbed level.

$$\frac{\partial^2}{\partial x^2}(\nabla^2\eta) + \frac{N^2}{U^2}\nabla_H^2\eta = 0; \quad N^2 = -\frac{g}{\rho_0}\frac{d\bar{\rho}}{dz} \tag{3}$$

To obtain a solution to (3) we represent η as a double Fourier integral

$$\eta(x,y,z) = \int\int_{-\infty}^{\infty} \hat{\eta}(k,l,z)e^{i(kx+ly)}\,dk\,dl \tag{4}$$

whereupon (3) becomes

$$\hat{\eta}_{zz} + m^2\hat{\eta} = 0 \tag{5}$$

with

$$m^2 = \frac{k^2+l^2}{k^2}\left(\frac{N^2}{U^2} - k^2\right) \tag{6}$$

With N^2 taken as constant the solution to (5) is

$$\hat{\eta}(k,l,z) = \hat{\eta}(k,l,0)e^{im(k,l)z} \tag{7}$$

For $k^2 > N^2/U^2$ the positive imaginary root of (6) must be chosen to eliminate the unphysical growth of the disturbance amplitude with height, and for $k^2 < N^2/U^2$ the sign of m must be chosen to be the same as the sign of k, in order to satisfy the radiation condition aloft.

The linearized lower boundary condition

$$\eta(x, y, z = 0) = h(x, y) \tag{8}$$

can be rewritten using the Fourier Transform of the mountain shape

$$\hat{h}(k, l) = \frac{1}{4\pi^2} \int \int_{-\infty}^{\infty} h(x, y) e^{-i(kx + ly)}\, dx\, dy \tag{9}$$

so that

$$\hat{\eta}(k, l, 0) = \hat{h}(k, l) \tag{10}$$

Finally then, from (4), (7), and (10),

$$\eta(x, y, z) = \int \int_{-\infty}^{\infty} \hat{h}(k, l) e^{\mathrm{im}(k, l)z}\, e^{i(kx + ly)}\, dk\, dl \tag{11}$$

with $m(k, l)$ given by (6) and $\hat{h}(k, l)$ given by (9). This (11) is the expression used by Wurtele (1957) in his study of the far-field dispersive waves behind a point source of vertical motion.

Now consider the bell-shaped mountain with circular contours

$$h(x, y) = \frac{h}{(r^2/a^2 + 1)^{3/2}}; \quad r = \sqrt{x^2 + y^2} \tag{12}$$

where "h" and "a" are the mountain height and horizontal scale. This shape was chosen by Crapper (1959) because of its particularly simple Fourier Transform (using (9) and (12))

$$\hat{h}(k, l) = \frac{1}{2\pi} ha^2\, e^{-a\kappa} \tag{13}$$

where $\kappa \equiv \sqrt{k^2 + l^2}$ is the magnitude of the horizontal wavenumber vector. The problem can be further simplified by using the hydrostatic approximation—setting the left-hand side of (1c) equal to zero. This reduces (6) to its hydrostatic form

$$m = \frac{N}{U} \frac{(k^2 + l^2)^{1/2}}{k}$$

or

$$m = \frac{N}{U \cos \psi} \tag{14}$$

where ψ is the angle of the horizontal wavenumber vector. This approximation is valid (now looking at (6)) for Fourier components with k such at $|k| < N/U$, and valid for the entire flow field if the mountain is broad enough that it generates only these small k components. From (13), this condition is

$$\frac{Na}{U} \gg 1 \tag{15}$$

which is that the horizontal scale of the mountain must be much larger than the distance of downwind drift during a buoyancy oscillation period. Choosing typical atmospheric values of $U = 10$ m/s and $N = 0.01$ s^{-1}, the condition (15) is that the horizontal scale must be much greater than 1 km. The hydrostatic model described herein should then be applicable to scales from 5 to 50 km. The flow over still broader mountains will be influenced by the Coriolis force, which is not included here. Non-hydrostatic flow and flow over other mountain shapes will be considered briefly in Sections 6 and 7.

Now introduce the non-dimensional variables

$$\hat{x} = x/a, \quad \hat{y} = y/a, \quad \hat{z} = z \frac{N}{U}$$
$$\hat{k} = ka, \quad \hat{l} = la, \quad \hat{\kappa} = \kappa a \tag{16}$$

so that (11), with (13) and (14), becomes

$$\eta(\hat{x}, \hat{y}, \hat{z}) = \frac{h}{2\pi} \int \int_{-\infty}^{\infty} e^{-\hat{\kappa}} e^{i\hat{z}/\cos\psi}\, e^{i(\hat{k}\hat{x} + \hat{l}\hat{y})}\, d\hat{k}\, d\hat{l} \tag{17}$$

which depends only on $\hat{x}$, $\hat{y}$, $\hat{z}$. Thus, in hydrostatic flow, the horizontal structure scales on "a" while the vertical structure scales on the length U/N. The hydrostatic flow obtained by numerically evaluating (17), using a two-dimensional FFT algorithm, is shown in Fig. 1. The details of the numerical technique are described in Appendix I. Very near the ground, the pattern of vertical displacement resembles the surface topography (12), as it must to satisfy the lower boundary condition (8). As we move slightly aloft ($\hat{z} = \pi/8$) a region of downward displacement forms over the lee slope of the mountain and extends some distance downstream. Further aloft, the region of down motion splits and widens to form a U-shaped region, with fluid particles returning smoothly to their undisturbed level downstream. As we continue to move aloft the region of down motion widens, moves upstream, and is replaced by a U-shaped region of upward displacement (i.e. $\hat{z} = \pi$). The general upstream shift of the identifiable regions is consistent with the radiation condition and the idea that the dis-

turbance is composed of vertically propagating mountain waves. At greater heights the zone of disturbance continues to broaden, the disturbance directly in the lee of the mountain disappears, the patterns of upward and downward motion become more wavelike, and the disturbance amplitude decreases.

To understand this flow in greater detail we will attempt to integrate (17) analytically. Note that the vertical wavenumber "m" given by the hydrostatic formula (14), depends only on the wavenumber direction ψ. Also, because the mountain (12) has circular contours, the Fourier Transform of the mountain shape depends only on the magnitude of the horizontal wavenumber κ. These features can be used to our advantage if we use cylindrical coordinates.

$$\hat{r} = (\hat{x}^2 + \hat{y}^2)^{1/2}; \quad \theta = \tan^{-1} \hat{y}/\hat{x}$$
$$\hat{\kappa} = (\hat{k}^2 + \hat{l}^2)^{1/2}; \quad \psi = \tan^{-1} \hat{l}/\hat{k} \tag{18}$$

so that (17) becomes

$$\eta(\hat{r}, \theta, \hat{z}) = \frac{h}{2\pi} \int_0^{2\pi} \int_0^{\infty} e^{-\hat{\kappa}} \, e^{i\hat{z}/\cos\psi} \, e^{j\hat{\kappa}\hat{r}\cos(\psi-\theta)} \times \hat{\kappa} \, d\hat{\kappa} \, d\psi \tag{19}$$

The integration over $\hat{\kappa}$ can be done exactly leaving

$$\eta(\hat{r}, \theta, \hat{z}) = \frac{h}{2\pi} \int_0^{2\pi} \frac{e^{i\hat{z}/\cos\psi} \, d\psi}{(1 - i\hat{r}\cos(\psi - \theta))^2} \tag{20}$$

The integration over ψ is apparently also possible but very tedious. Instead we will derive asymptotic formulae describing the flow far from the mountain ($\hat{r} \gg 1$), high above the mountains ($\hat{z} \gg 1$), and close to the ground ($\hat{z} \approx 0$).

3. The flow aloft

To obtain an approximation to (20) valid far from the mountain, we note that with $\hat{r} \gg 1$ the major contributions to the integral come near $\psi - \theta = \pm\pi/2$ where $\cos(\psi - \theta)$ is small. With this as a basis the following asymptotic formulae are obtained (see Appendix II for details) for $\hat{r} \gg 1$ upstream

$$(x < 0) \quad \eta(\hat{r}, \theta, \hat{z}) = 0 + O\left(\frac{1}{\hat{r}^2}\right) \tag{21a}$$

downstream

$$(x > 0) \quad \eta(\hat{r}, \theta, \hat{z}) = \frac{2h}{\hat{r}} [\beta e^{-\beta}] \cos\left(\frac{\hat{z}}{\sin\theta}\right) + O\left(\frac{1}{\hat{r}^2}\right) \tag{21b}$$

with $\beta \equiv \hat{z}\hat{x}/\hat{y}^2$.

In dimensional form (21b) is

$$\eta(x, y, z) = 2h \frac{a}{r} [\beta e^{-\beta}] \cos\left(\frac{Nz}{U \sin\theta}\right) + O\left(\frac{a}{r}\right)^2 \tag{22}$$

with $\beta \equiv Nzax/Uy^2$.

This curious formula correctly describes the qualitative nature of the exact numerical results (shown in Fig. 1) beyond $r/a \approx 3$ and gives a quantitatively accurate representation beyond $r/a \approx 10$ or so. We remark in passing that the derivation of (21) is not a direct application of the method of stationary phase such as used by Wurtele and Crapper. The method of stationary phase cannot be used in the hydrostatic problem as one of the "principal curvatures" vanishes. This is seemingly connected with the fact that the hydrostatic lee waves, being in some sense less dispersive than the non-hydrostatic waves, decay as $1/r$ instead of $1/r^2$.

The pattern defined by (21) or (22) is most easily described by breaking these formulae into three factors. The local wave-like behavior is given from the factor cos $(Nz/U \sin\theta)$. Note that at a fixed height z, this depends only on θ and thus the phase lines are radii passing back through the origin where the mountain is located. The phase surfaces tilt upstream and outward with increasing height. The amplitude factor $[\beta e^{-\beta}]$ has a maximum at

$$\beta \equiv \frac{Nzax}{Uy^2} = 1 \tag{23}$$

and thus the wave energy will be concentrated in regions where (23) is nearly met. At a fixed z, (23) represents a parabola with vertex at the origin and trailing downstream. This parabola becomes wider as z increases. The a/r factor describes the general decay of the disturbance away from the mountain. All three of the qualitative features; the radial, outward tilting phase lines, the concentration of the disturbance along parabolas which widen with height, and the decay away from the mountain, are evident in retrospect in the numerical solutions

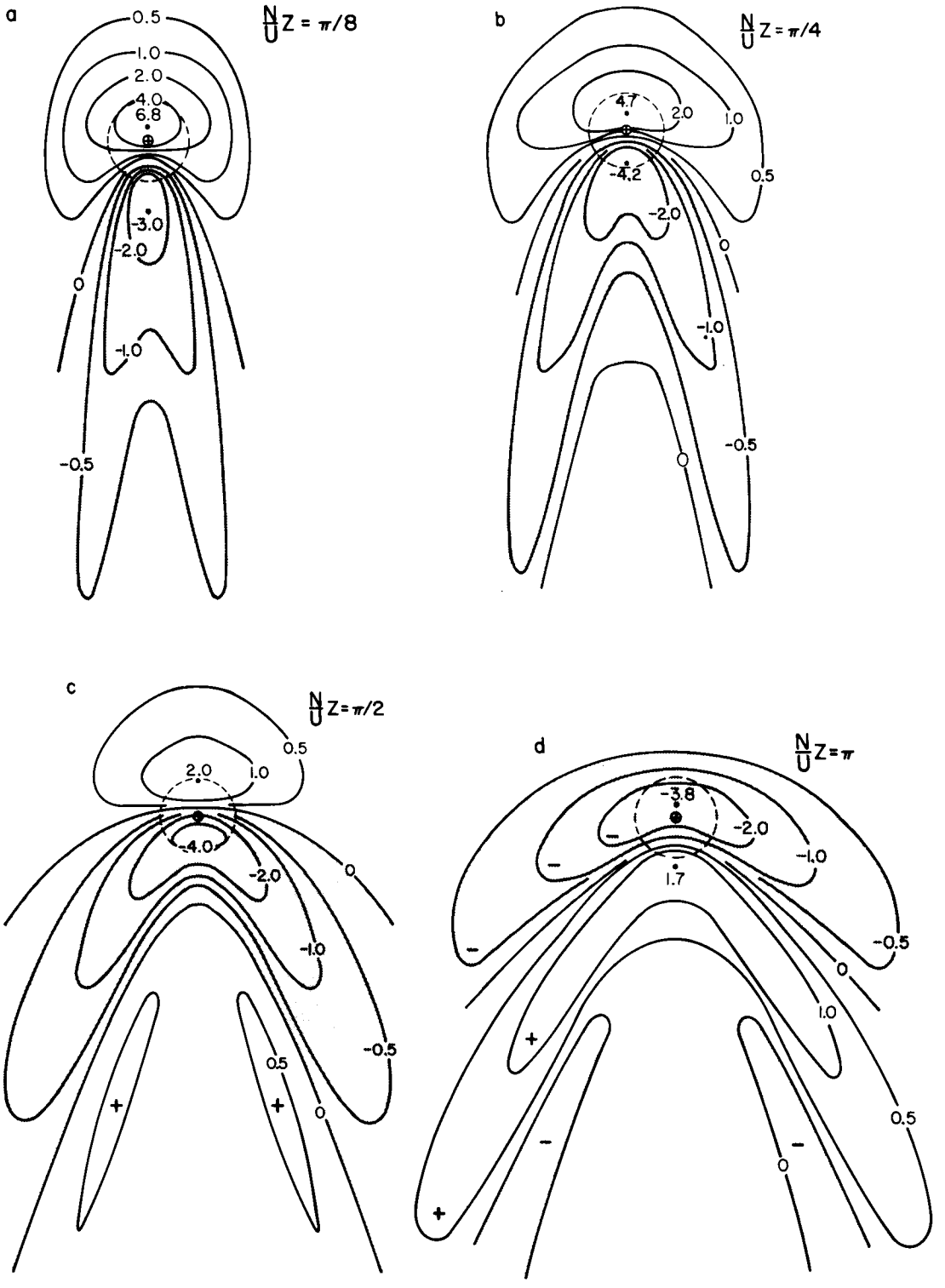
a
NZ/U = π/8
0.5
1.0
2.0
4.0
6.8
-3.0
-2.0
0
-1.0
-0.5
b
NZ/U = π/4
4.7
2.0
1.0
-4.2
0.5
-2.0
0
-1.0
-0.5
0
c
NZ/U = π/2
0.5
2.0
1.0
-4.0
-2.0
0
-1.0
-0.5
0.5
+
+
0
d
NZ/U = π
-3.8
-2.0
-1.0
1.7
-0.5
0
1.0
0.5
+
-
-
0
-

shown in Fig. 1. It remains to explain these features of the flow physically, and this can be done using group velocity arguments.

The dispersion relation for internal gravity waves in a stagnant Boussinesq fluid is

$$\sigma = \pm \left(\frac{N^2(k^2 + l^2)}{k^2 + l^2 + m^2} \right)^{1/2} \tag{24}$$

where k, l, m are the x, y, z directed components of the total wavenumber vector. With the hydrostatic approximation this becomes

$$\sigma = \frac{\pm N(k^2 + l^2)^{1/2}}{m} \tag{25}$$

The efficiency and direction of transport of wave energy through the fluid by pressure–velocity correlations, are described by the group velocity components.

$$C_{g_x} = -\frac{\partial \sigma}{\partial k} = -\frac{N(k^2 + l^2)^{-1/2} k}{m} \tag{26a}$$

$$C_{g_y} = -\frac{\partial \sigma}{\partial l} = -\frac{N(k^2 + l^2)^{-1/2} l}{m} \tag{26b}$$

$$C_{g_z} = -\frac{\partial \sigma}{\partial m} = +\frac{N(k^2 + l^2)^{1/2}}{m^2} \tag{26c}$$

For steady waves on a mean current we replace σ with the intrinsic frequency Uk so that (25) gives

$$m = \pm \frac{N}{U} \frac{(k^2 + l^2)^{1/2}}{k} \tag{27}$$

(cf. (14)). The components of the group velocity in fixed coordinates is then (adding U to (26a) and using (27))

$$C_{g_x} = U \frac{l^2}{k^2 + l^2} \tag{28a}$$

$$C_{g_y} = -U \frac{kl}{k^2 + l^2} \tag{28b}$$

$$C_{g_z} = \frac{U^2 k^2}{N(k^2 + l^2)^{1/2}} \tag{28c}$$

In earth fixed coordinates, wave energy propagates from the energy source (i.e. the mountain) along straight lines with slopes

$$x/z = C_{g_x}/C_{g_z} \tag{29a}$$

$$y/z = C_{g_y}/C_{g_z} \tag{29b}$$

$$y/x = C_{g_y}/C_{g_x} \tag{29c}$$

Slope (29c) is evaluated using (28a, b) to give

$$y/x = -k/l \tag{30}$$

which is the geometric condition that the phase lines passing through the point (x, y) are radial lines from the origin (cf. eq. (22) and Fig. 1). This is shown schematically in Fig. 2.

Using (29a, b) and (28) gives

$$y^2 = \frac{N}{U} z(k^2 + l^2)^{-1/2} x \tag{31}$$

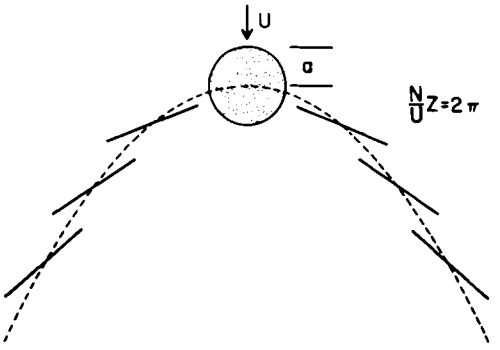

Fig. 2. A schematic representation of the far-field hydrostatic wave pattern in accordance with the asymptotic expression (21b) and the group velocity arguments which lead to (30) and (33). At any height z, the wave energy is concentrated near the parabola $y^2 = Nzax/U$ (shown dashed). At higher altitudes this parabola becomes wider—a trend which is apparent in Fig. 1. The phase lines, i.e., the wave crests and troughs, are radii which point back toward the mountain.

Fig. 1. The vertical displacement $\eta(x, y, z)$ at various levels associated with hydrostatic stratified flow over an isolated bell-shaped mountain (12) with $h = 10$. Regions of downward displacement are shaded. The cross ⊕ marks the position of the mountain top. The dashed circle is the topographic contour at $r = a$. These patterns are computed by evaluating (17) numerically using a two-dimensional FFT. Near the ground the vertical displacement approaches the topographic shape but as we move aloft $(N/U)z = \pi/8$) a region of down motion develops in the lee. Further aloft ($(N/U)z = \pi/4$ and $\pi/2$) this region splits and widens to form a U-shape. Still further aloft ($(N/U)z = \pi$) the region of down motion has moved upstream and a U-shaped region of upward displacement has formed in the lee. The qualitative nature of this flow is explained by the asymptotic analysis and the group velocity arguments in the text.

We expect that the mountain will primarily generate waves with the magnitude of the horizontal wavenumber equal to the inverse of the mountain width scale.

$$\sqrt{k^2 + l^2} = \frac{1}{a} \tag{32}$$

Substituting (32) into (31) gives

$$y^2 = \frac{Nzax}{U} \tag{33}$$

which is identical to the direct asymptotic result (23). Waves which satisfy (32) can only propagate to regions in space (x, y, z) which satisfy (33). Looked at in more detail, those waves with phase fronts nearly perpendicular to the incoming flow (i.e. $k \gg l$) will propagate vertically and their wave energy will be found directly above the mountain—as in two-dimensional hydrostatic flow. The waves with phase fronts at an appreciable angle to the flow (i.e. $k \approx l$) will propagate upwards, outwards, and downstream. The wave packet trajectories become very shallow and oriented nearly downstream in the limit of $k/l \to 0$. These waves are primarily advected downstream by the mean flow (see (28a)). The surface composed of all of these radial trajectories, is simply (33).

The region of small y and z, but large x, i.e. the far-field "wake" of the mountain, seems to be singular in some sense. The asymptotic solution (22) behaves violently in this region. Group velocity arguments indicate that the Fourier component which control the flow in the wake are those whose phase fronts nearly parallel the incoming flow, so that their intrinsic frequency Uk is very small. The vertical wavenumber (14) approaches infinity for these waves, and large vertical gradients are expected—perhaps leading to viscous effects or turbulence in a real flow.

There is an analogy between the singular wake in three-dimensional flow and the critical level in two-dimensional flow with a mean velocity $U(z)$ that decreases to zero at some height (Booker and Bretherton, 1967). Both regions, the singular wake region and the critical layer, are controlled by waves with vanishing intrinsic frequency and thus infinite vertical wavenumber.

The singular wake region will be discussed again when we describe the flow near the ground.

The flow directly above the mountain at great heights can be determined from an asymptotic evaluation of (20) for $\hat{z} \equiv z(N/U) \gg 1$ while $\hat{r} \equiv r/a = O(1)$. The result from Appendix IV is

$$\eta(x, y, z) \cong \frac{h}{\sqrt{\pi}} \sqrt{\frac{U}{Nz}} \frac{1}{(1 + \hat{x}^2)^2} \times [(1 - 2\hat{x} - \hat{x}^2) \cos \hat{z} - (1 + 2\hat{x} - \hat{x}^2) \sin \hat{z}] \tag{34}$$

As with the earlier asymptotic results, this formula compares well with the exact numerical solution in the appropriate region. Equation (34) describes a field of vertically propagating waves with phase fronts perpendicular to the incoming flow. This is consistent with the progressive spreading of the wave fronts aloft, described by (23) and seen in Fig. 1. The phase lines tilt upstream with height just as they do in two-dimensional flow. Unlike two-dimensional hydrostatic flow, the amplitude of the displacements given by (34), decay upwards as $z^{-1/2}$. In a compressible atmosphere, this decay would eventually be overwhelmed by the amplification ($\sim e^{+z/2H}$) due to the decrease of density with height and the waves would eventually steepen and break down by overturning or by flow instability.

4. The flow near the ground

The flow at and near the ground is of particular interest, and not difficult to obtain. Integrals of the form (20) can be evaluated easily by contour integration in the complex plane, if the troublesome $e^{i\hat{z}/\cos\psi}$ factor is reduced to unity by setting $\hat{z} = 0$. First we will evaluate the surface pressure field. Combining (1e) with the hydrostatic form of (1c) and integrating vertically gives

$$p'(x, y, z) = -g \frac{d\bar{\rho}}{dz} \int_z^\infty \eta(x, y, z')\, dz' \tag{35}$$

where the perturbation pressure at infinity is assumed zero, due to the decay of the wave field aloft. Using (20) in (35) and setting $z = 0$ gives

$$p'(x, y, 0) = g \frac{d\bar{\rho}}{dz} \frac{U}{N} \frac{h}{2\pi} \int_0^{2\pi} \frac{\cos\psi\, d\psi}{i\left(1 - i\frac{r}{a}\cos(\psi - \theta)\right)^2} \tag{36}$$

This can be evaluated by contour integration (see Appendix III for details) to give

$$p'(x, y, 0) = -\rho_0 NUh \frac{x/a}{(1 + r^2/a^2)^{3/2}} \tag{37}$$

which is shown in Fig. 3. High pressure is found on the windward slope of the mountain and low pressure on the lee side. As in the two-dimensional case, this pressure asymmetry, and the resulting mountain drag, are associated with generation of vertically propagating waves. Bernoulli's equation, linearized in the form

$$p' + \rho_0 Uu' = 0 \tag{38}$$

together with (37), give the downstream velocity perturbation

$$u'(x, y, 0) = hN \frac{x/a}{(1 + r^2/a^2)^{3/2}} \tag{39}$$

The lateral velocity perturbation can be found by integrating (1b)

$$v'(x, y, 0) = \frac{-1}{\rho_0 U_0} \int_{-\infty}^{x} p'_y(x, y, 0)\, dx \tag{40}$$

Evaluating (40) with P' from (37) gives

$$v'(x, y, 0) = hN \frac{y/a}{(1 + r^2/a^2)^{3/2}} \tag{41}$$

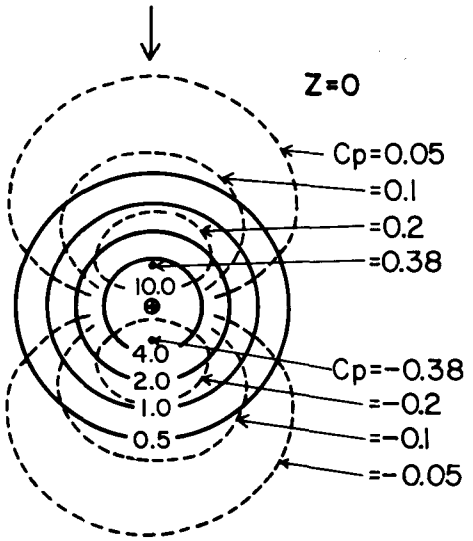

Fig. 3. The topographic contours of the bell-shaped mountain given by (12) with $h = 10$ (shown in solid lines) and the isobars of perturbation surface pressure for hydrostatic flow given by (37) (shown dashed). The pressure coefficient is defined as $c_p \equiv p'/\rho UNh$ and is also equal to $-u'/Nh$ using (38).

The lateral displacement δ is found from (41) by again integrating downstream

$$\delta(x, y, 0) = \frac{1}{U} \int_{-\infty}^{x} v'(x, y, 0)\, dx \tag{42}$$

which is

$$\delta(x, y, 0) = \frac{hN}{U} \frac{y}{1 + y^2/a^2} \left(1 + \frac{x/a}{(1 + r^2/a^2)^{1/2}}\right) \tag{43}$$

The lateral displacement of the surface streamlines given by (43) is shown in Fig. 4. The lateral displacement of the low level fluid is connected with the pressure field in the following way. As a fluid particle to the right of the x-axis approaches the mountain, it experiences high pressure on its left, and therefore curves to the right. Abreast of the mountain it has an outward lateral velocity but feels no lateral pressure gradient and thus its path is not curved. Downstream of the mountain, the particle feels low pressure on the left and thus curves to the left, eventually returning to its original direction. There is, however, a permanent outward deflection to those streamlines which pass by in the vicinity of the mountain.

Near the surface, the pattern of vertical displacement can be represented as a Taylor series

$$\eta(x, y, z) \approx \eta(x, y, 0) + \eta_z \cdot z + \ldots \tag{44}$$

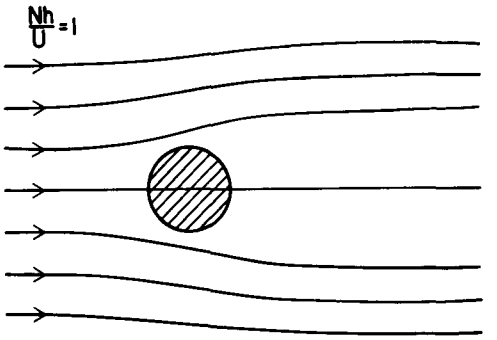

Fig. 4. The surface streamlines (given by (43)) of hydrostatic flow past an isolated bell-shaped mountain (12). The circle represents a topographic contour at $r = a$. Except on the centerline, the fluid is deflected away from the mountain by the surface pressure field shown in Fig. 3. This deflection is permanent, as shown, only right at $z = 0$. At any finite height, the streamlines eventually return to their original position.

where from (8), $\eta(x, y, 0) = h(x, y)$. The quantity η_z represents the increase (or decrease if η_z is negative) of the vertical distance between surfaces of constant density (isentropic surfaces in the atmosphere). This quantity can be computed by using the conservation of mass flux along a stream tube

$$\frac{d}{dx}\left(\eta_z + \delta_y + \frac{u'}{U}\right) = 0 \tag{45}$$

with (39) and (43), or by taking the vertical derivative of (20) and evaluating it at $z = 0$

$$\eta_z = \frac{hN}{2\pi U}\int_0^{2\pi} \frac{i\,d\psi}{\cos\psi\left(1 - i\frac{r}{a}\cos(\psi - \theta)\right)^2} \tag{46}$$

Evaluation of (46) by contour integration yields

$$\eta_z(x, y, 0) = \frac{hN}{U}\left(\frac{-1}{\hat{y}^2 + 1}\right)$$
$$\left[1 + \frac{\hat{x}(1 - \hat{y}^2)}{(\hat{y}^2 + 1)(\hat{r}^2 + 1)^{1/2}} - \frac{2\hat{y}^2}{(\hat{y}^2 + 1)} + \frac{\hat{x}}{(\hat{r}^2 + 1)^{3/2}}\right] \tag{47}$$

This formula, (47), when used in (44), very accurately reproduces the numerical results for η at low levels (for example Fig. 1a) except far downstream directly in the lee of the mountain—i.e., in the singular wake region. As one moves downstream in this region the truncated Taylor series (44) is useful to progressively smaller altitudes. This is connected with the fact that this region is controlled by Fourier components with large vertical wavenumbers.

Through the mass flux condition (45), the vertical displacement described by (47) can be connected to the increase or decrease in downstream velocity u' and to the lateral streamline divergence δ_y. Along the centreline of the mountain the low layers thicken and then thin, in response to the velocity minimum and maximum. Added to this is a permanent thinning of the low layers—i.e. a *sinking of warm air from aloft*—to compensate for the horizontal divergence shown in Fig. 4.

The permanent lateral deflection of the low level streamlines (Fig. 4) and the compensating downward deflections (Fig. 5) are not artifacts of the hydrostatic approximation. In fact, a simple expression can be derived for the lateral deflection far

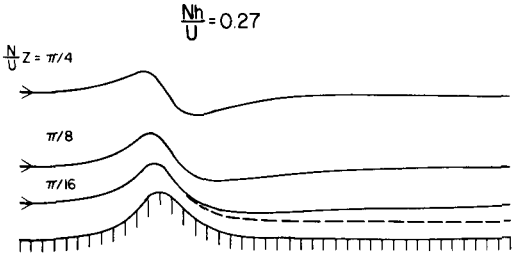

Fig. 5. The vertical displacements of the streamlines in the center plane $y = 0$ for hydrostatic flow over an isolated bell-shaped mountain (12) as computed numerically. The approximation given by (44) and (47) is shown dashed. The phase lines tilt upstream as in two-dimensional flow but the wave amplitude decreases with height. The long-lasting downward deflection behind the mountain is associated with the horizontal divergence shown in Fig. 4, rather than an increased velocity.

downstream $\delta(x = \infty, y, z = 0)$ for arbitrary mountain shape, and without using the hydrostatic assumption. From (1b), (1c), and (1e) a relationship between the Fourier Transforms of v' and η can be obtained in the form

$$\hat{v}(k, l, z) = f(k, l)\,\hat{\eta}(k, l, z) \tag{48}$$

and at the ground—using (10)

$$\hat{v}(k, l, 0) = f(k, l)\,\hat{h}(k, l) \tag{49}$$

From the property of the Fourier Transform

$$\hat{v}(0, l, 0) = \frac{1}{4\pi^2}\int_{-\infty}^{\infty}\left[\int_{-\infty}^{\infty} v(x, y, 0)\,dx\right]e^{-ily}\,dy \tag{50}$$

where the integral in brackets is proportional to the permanent lateral deflection according to

$$\int_{-\infty}^{\infty} v(x, y, 0)\,dx = U \cdot \delta(\infty, y, 0) \tag{51}$$

Note also that

$$\hat{h}(0, l) = \frac{1}{4\pi^2}\int_{-\infty}^{\infty} A(y)e^{-ily}\,dy \tag{52}$$

where

$$A(y) \equiv \int_{-\infty}^{\infty} h(x, y)\,dx \tag{53}$$

is the area of a downstream cross-section through the mountain. To compute $f(k, l)$ as $k \to 0$, we need only its hydrostatic form

$$f(k, l) = \frac{-ilN^2}{Ukm} \tag{54}$$

with m given by (14), which gives

$$f(0, l) = -iN \operatorname{sgn}(l) \tag{55}$$

Now using (49), (50), (51), (52), (53), and (55) we can relate the y- transform of $A(y)$ (call this $\hat{A}(l)$) and the y-transform of $\delta(\infty, y, 0)$ (call this $\hat{\delta}(l)$);

$$\hat{\delta}(l) = -i \frac{N}{U} \operatorname{sgn}(l)\, \hat{A}(l) \tag{56}$$

This equation can be interpreted to say that the surface flow will be permanently deflected away from regions with large $A(y)$ and will tend to converge downstream of small $A(y)$ areas. This deflection will be absent (still looking at (56)) only when the ridge cross-sectional area ($A(y)$) is independent of y or when the fluid is not stratified.

We reemphasize the point that while the lateral deflections (56) and the associated vertical motions may be evident some distance downstream, they are confined to a progressively shallower region. Far downstream, they will presumably be modified by non-ideal processes brought about by the singular nature of the wake.

5. The breakdown of linear theory and the criterion for flow around the mountain

As the parameter hN/U increases, the disturbance amplitude increases in relation to the background flow and when hN/U become of order one, the linear theory is no longer valid. There are several criteria which can be used to mark the breakdown of linear theory. For example, (a) the perturbation velocity component u', as given by (39), first becomes equal but opposed to U, bringing the total flow to a halt on the windward slope at

$$(x, y, z) = (-0.7a, 0, 0)$$

and this occurs when

$$\frac{hN}{U} \approx 3 \tag{57}$$

(b) Part of the surface level flow deflects laterally to avoid the mountain when δ, given by (43) and evaluated at $x = 0$, becomes equal to the mountain width "a". This occurs at $|y| = a$ when

$$\frac{hN}{U} = 1 \tag{58}$$

(c) The vertical distribution of density (or potential temperature) collapses and the stability becomes infinite when η_z, given by (47), equals -1. This first occurs on the centerline, downstream of the mountain at $x = 1.4a$, when

$$\frac{hN}{U} = 1/2.09 \tag{59}$$

and occurs downstream of this point all along the x-axis when

$$\frac{hN}{U} = 1/2 \tag{60}$$

This early collapse of the potential temperature surfaces in the wake region is associated with the divergence shown in Fig. 4 and is an indication that the three-dimensional flow studied herein is more sensitive to finite amplitude effects than the flow over an infinite ridge.

The criteria discussed above can be compared with the blocking criterion of Sheppard (1956). Consider a surface streamline leading to the mountain peak. Along this streamline Bernoulli's equation gives

$$P_{-\infty} + \tfrac{1}{2}\rho_0 U_{-\infty}^2 = P_T + \tfrac{1}{2}\rho_0 U_T^2 + g\rho_0 h_T \tag{61}$$

where the subscripts $-\infty$ and T refer to points far upstream and at the mountain top respectively. In analogy with an energy-conserving frictionless puck sliding on an uneven surface, Sheppard assumed that the flow would reach its lowest speed at the mountain top and that the onset of blocking would be signaled by U_T going to zero. He further assumed that the perturbation pressure p' at the top would be zero (this agrees with (37)), so that

$$P_T = P_{-\infty} + g\left[\rho_0 - 1/2 \frac{\partial \rho}{\partial z} h_T\right] h_T \tag{62}$$

From (61) and (62), the blocking condition is

$$\frac{hN}{U} = 1 \tag{63}$$

The appearance of the same parameter—i.e. the inverse Froude number hN/U—does not imply that Sheppard's parcel argument is equivalent to the analyses leading to (57)–(60), as this grouping follows from dimensional analysis. In fact, the continuum theory, with the radiation condition aloft, predicts that the minimum speed will occur

on the windward slope (see (39) and (57)) not at the mountain top.

If one wishes to construct an energy argument for blocking, which is consistent with the results of linear theory, one must argue as follows. If the air is able to flow over the obstacle, as is assumed in (8), then gravity waves will be produced which will radiate energy away at a rate

$$\text{drag} \cdot U \sim \rho U N h^2 a \cdot U \tag{64}$$

whereas the kinetic energy incident on the mountain is

$$\sim [\tfrac{1}{2}\rho U^2] \cdot U h a \tag{65}$$

The rate of energy loss (64) will exceed the supply (65) when

$$\frac{hN}{U} > O(1) \tag{66}$$

and the flow must then avoid the mountain. Of course this line of reasoning implicitly assumes that only the kinetic energy incident on the mountain is relevant, but in fact the mountain drag may act on an entirely different region of the flow.

When the Froude number is very small, $hN/U \gg 1$, the stratification dominates to the extent that fluid particles pass around the mountain while remaining in horizontal planes. If the mountain has circular topographic contours of radius "$a(z)$", the pressure field at each level, calculated from potential theory, is of the form

$$p'(r, \theta, z) = \frac{1}{2}\rho U^2 f(r/a(z), \theta) \tag{67}$$

Unless the mountain has vertical sides, there will be a vertical pressure gradient (using (67)).

$$p'_z = \frac{1}{2}\rho U^2 f'(r/a, \theta)\left(\frac{-r}{a^2}\right)\frac{da}{dz} \tag{68}$$

Drazin (1961) has pointed out that this vertical pressure gradient can be hydrostatically balanced in the presence of small vertical deflections η. From (35)

$$p'_z = g\frac{d\bar{\rho}}{dz}\eta \tag{69}$$

The horizontal flow approximation which led to (67), is presumed to be valid if the vertical deflections predicted from (68) and (69) are so small that the parcels do not rise to a level where the mountain is significantly narrower—i.e.

$$\frac{\eta}{a}\frac{da}{dz} \ll 1 \tag{70}$$

Using (68) and (69), this becomes

$$\left(\frac{U}{N}\frac{1}{a}\frac{da}{dz}\right)^2 \ll 1 \tag{71}$$

The criterion can be applied to the mountain as a whole by choosing

$$\frac{1}{a}\frac{da}{dz} = \frac{1}{h}$$

so that (71) is

$$\left(\frac{U}{Nh}\right)^2 \ll 1 \tag{72}$$

The condition (71) will always be violated locally at the top of the mountain ($a(z) \to 0$) unless the peak is cusped.

It is curious to note that both the small and large Froude number theories predict flow around and vertical displacements but the qualitative nature of these predictions are quite different. The small Froude number theory predicts pressure and vertical displacements which have fore–aft symmetry. There are no mountain waves and no wave drag, and the horizontal displacements are temporary. The large Froude number theory (i.e. linear theory) predicts asymmetric pressure and vertical displacements associated with the generation of waves. The lateral deflection to avoid the mountain increases downstream and becomes permanent. It seems likely that the range of validity of these two theories, and the transition between them, could be elucidated by a well-designed laboratory or numerical experiment. It is possible, however, that these flows may be quite sensitive to viscosity, either due to separation of the flow in the low Froude number case, or to non-ideal behavior in the singular wake region of the large Froude number case. Riley et al. (1975) find in experiments at low Froude number that the flow splits to avoid the mountain and this horizontal deflection persists some distance downstream. When the Froude number is increased enough so that vertical displacements become evident, those displacements are strongly asymmetric with slight lifting on the

windward slope and stronger sinking in the lee. They suggest that this can be accounted for by lee-side boundary layer separation occurring in each horizontal plane—thus altering the pressure distribution (67). Another possibility is just to realize that the observations of Riley et al. are qualitatively consistent with the predictions of inviscid linear theory as discussed in this paper.

A further problem in interpretation arises from the use of steep mountains ($h/L \sim 1$) in the laboratory experiments. In this case the two dimensionless numbers U/Nh and U/NL (h and L are the vertical and horizontal scales of the topography) are the same order. As U/N increases, for fixed h and L, the flow is more able to rise over the mountain but at the same time vertical accelerations become important (see eq. (15)). Thus in order to model the transition from $U/Nh \ll 1$ to $U/Nh \gg 1$, while maintaining hydrostatic balance, a realistically gentle mountain ($h/L \ll 1$) must be used.

6. The flow past a long ridge

To determine the flow over more complicated terrain, we can either use the numerical FFT technique, described in Appendix I, or else superpose a number of solutions arising from the simple shape (12). It is particularly interesting to do this for a long ridge, as this helps to explain how the flow approaches the much studied two-dimensional limit. As shown in Fig. 6, there is parabolic zone trailing from the end of the ridge in which the transition between the undisturbed region, to the sides of the ridge and the decaying two-dimensional disturbance behind the ridge, occurs. This parabola becomes broader with height and is well described by (23). The reason for the shape of this region is clarified by considering that each segment of the ridge produces parabolic zones of disturbance as described by (21). Working backwards, the two-dimensional disturbance at any point in the lee ($x > 0$, y, z) can be thought of as a sum of the disturbances emanating from two short segments of the ridge, found by tracing the parabolas to the left and right upstream. For points within the parabola coming from the ridge end, only one ridge segment is effective and the disturbance departs from two dimensionality. For a ridge of length "L" and width "a", two-dimensional theory is valid in the lee near the ground but becomes inapplicable further downstream or aloft as the parabolas from the ridge ends widen. The ridge width "a" enters directly in this criterion as the width of the parabola is proportional to "a" (see (23)).

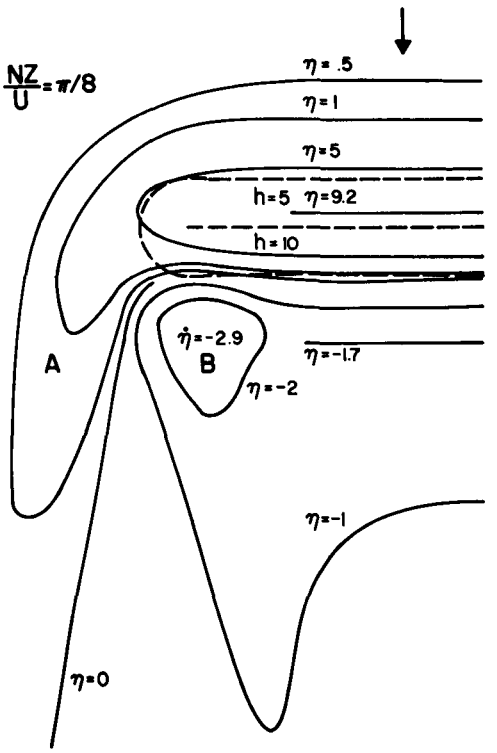

Fig. 6. The pattern of vertical displacement (η) near the end of a long ridge, at a height z such that $(N/U)z = \pi/8$. The ridge is of Gaussian shape $h(x, y) = 10 \cdot e^{-(d/a)^2}$ where d is the distance from ridge crest line. The ridge crest line (i.e. $h = 10$) and the $h = 5$ contour are shown dashed. Away from the ridge end, the flow is as if the ridge were infinitely long. Downstream of the end of the ridge there is a complicated transition region which widens downstream and aloft according to (23). The raised and depressed regions, A and B, are associated with horizontal convergence and divergence occurring as the low-level air, passing near the ridge end, is deflected laterally away from the ridge.

The criteria for two-dimensional flow *upstream* of a finite ridge is less well defined. This is so because the disturbance upstream of an isolated mountain (see (21)) decays more rapidly but is not confined to parabolic zones. The vertical displacements upstream of an infinite ridge are just as

strong as those downstream, but must be thought of as emanating from long portions of the ridge.

There is, of course, no lateral deflection of the surface streamlines in the infinite ridge case, but near the ends of a finite ridge the flow will be deflected away from the ridge. To compensate for this, there will be zones of upward and downward displacement just in the lee of the ridge end (Fig. 6).

If the mean flow is obliquely inclined to the ridge, the disturbance can be analyzed in a similar way noting only that the parabolic zones of influence are aligned with the mean flow and are not necessarily perpendicular to the ridge. In regions where the flow is two dimensional, the vertical wavenumber N/U must be computed from the component of U which is perpendicular to the ridge.

7. Non-hydrostatic flow

The theoretical progress reported in this paper is due primarily to the simplification which results from the hydrostatic approximation. The numerical FFT technique, however, can be used with (6) (instead of (14)) to construct solutions without this approximation. The non-hydrostatic flow ($U/Na = 1$) over the mountain (12) is shown in Fig. 7—to be compared with the hydrostatic flow in Fig. 1. The U-shaped region of down motion is similar in both cases but in the non-hydrostatic solution the fluid particles undergo a damped oscillation instead of recovering smoothly downstream. The wavelength of these oscillations rapidly approaches $\lambda = 2\pi U/N$, corresponding to a pure buoyancy oscillation. These trailing lee waves have been discussed by Wurtele (1957) and Crapper (1959, 1962).

In the limit $U/Na \gg 1$, the buoyancy forces are unimportant and no mountain waves are generated. The integral (11) can easily be evaluated with (13) and with (6) reduced to the form

$$m = i\kappa \tag{73}$$

to give

$$\eta(x, y, z) = \frac{ha^3}{(r^2 + (a + z)^2)^{3/2}} \tag{74}$$

This flow (74), is identical to the potential flow past a spherical doublet placed below the $z = 0$ plane.

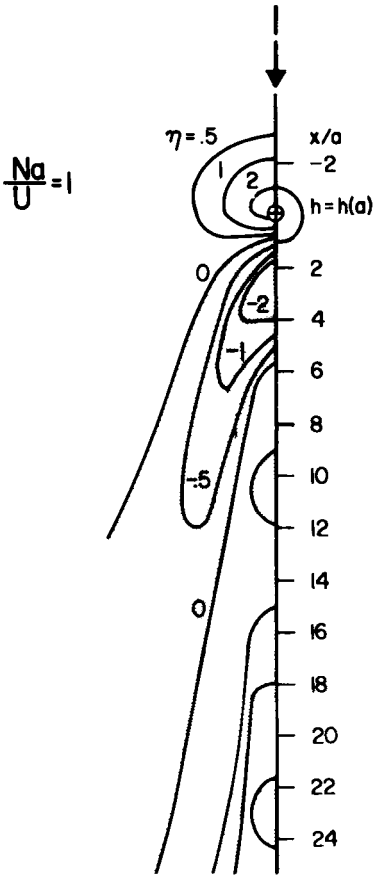

Fig. 7. The non-hydrostatic flow past an isolated bell-shaped mountain (12) as computed numerically for the case $Na/U = 1$. The vertical displacements at the height $Nz/U = \pi/4$ are shown. The lifting over the windward slope and the U-shaped region of downward displacement in the lee, are similar to the hydrostatic flow in Fig. 1b. The periodic lee waves apparent in this figure are inherently non-hydrostatic. Their wavelength approaches $\lambda = 2\pi(U/N)$, corresponding to parcels oscillating at the buoyancy frequency N while being advected downstream.

The transition from irrotational flow (74) to buoyancy dominated hydrostatic flow, described herein for an isolated mountain, is similar in many respects to the corresponding study of Queney (1947) for an infinite ridge. (This transition and other aspects of mountain flow dynamics are reviewed by Smith, 1979.)

8. Discussion

Perhaps the most interesting aspect of the foregoing is the linear theory prediction that the

low level flow has a tendency to split to avoid the mountain. This lateral deflection persists downstream and passes into the singular wake region. The horizontal divergence is compensated for by the descent of warm air from aloft. The general nature of these predictions are not strongly dependent on the hydrostatic assumption or on the choice of mountain shape, but are closely associated with the generation of three-dimensional mountain waves. The blocking criterion of Sheppard (1956), using a parcel argument, does not seem useful in this context. Furthermore, the linear theory result is quite distinct from the low Froude number result of Drazin (1961).

As we move aloft, the region of descent behind the mountain splits and becomes part of a three-dimensional field of vertically propagating mountain waves. These waves are primarily confined to parabolas which trail from the mountain and widen with height. The strongest waves are found directly over the mountain. The energy density of these waves decays upward due to the three dimensionality but, due to the decrease in air density, the wave amplitude will increase and wave breakdown must eventually occur.

9. Acknowledgements

The author gratefully acknowledges the helpful comments of Robert Hall and George Veronis of Yale University, and the careful review of C. D. McGregor. The Fast Fourier Transform algorithm used in this study was supplied by the Computer Facility of the National Center for Atmospheric Research. This research was supported under grant ATM-7722175 from the National Science Foundation.

10. Appendix I—Numerical techniques

The two-dimensional FFT algorithm numerically computes the complex finite Fourier series defined by

$$\hat{F}(J_1, J_2) = \sum_{1}^{N_1} \sum_{1}^{N_2} F(I_1, I_2) \cdot \exp\left(\frac{2\pi(I_1 - 1)(J_1 - 1)}{N_1} + \frac{2\pi(I_2 - 1)(J_2 - 1)}{N_2} \right) \quad \text{(AI.1)}$$

Knowing $\hat{F}(J_1, J_2)$, the original function $F(I_1, I_2)$ can be returned by using the inverse FFT to compute

$$F(I_1, I_2) = \frac{1}{N_1 N_2} \sum_{1}^{N_1} \sum_{1}^{N_2} \hat{F}(J_1, J_2) \cdot \exp\left(\frac{-2\pi(J_1 - 1)(I_1 - 1)}{N_1} + \frac{-2\pi(J_2 - 1)(I_2 - 1)}{N_2} \right) \quad \text{(AI.2)}$$

To evaluate (11) in the text)

(1) The mountain shape $h(x, y)$ is represented as an array $h(I_1, I_2)$ by sampling with an interval Δx and Δy.

(2) The FFT algorithm is called to evaluate $\hat{h}(J_1, J_2)$ according to (AI.1).

(3) Each Fourier coefficient $\hat{h}(J_1, J_2)$ is multiplied by $\exp(i \cdot m(J_1, J_2) \cdot z)$. In computing the vertical wavenumber "m", eq. (6) or (14) is used with the horizontal wavenumbers k, l computed from

$$k = \frac{2\pi(J_1 - 1)}{N_1 \cdot \Delta x} \quad \text{if} \quad J_1 \leq \frac{N_1}{2} + 1$$

or

$$k = \frac{-2\pi(N_1 + 1 - J_1)}{N_1 \cdot \Delta x} \quad \text{if} \quad J_1 \geq \frac{N_1}{2} + 1$$

and

$$l = \frac{2\pi(J_2 - 1)}{N_2 \cdot \Delta y} \quad \text{if} \quad J_2 \leq \frac{N_2}{2} + 1$$

or

$$l = \frac{-2\pi(N_2 + 1 - J_2)}{N_2 \cdot \Delta y} \quad \text{if} \quad J_2 \geq \frac{N_2}{2} + 1$$

In this way, the high wavenumbers $J \geq (N/2) + 1$, which have non-zero coefficients because of aliasing, are treated as small negative wavenumbers—and the utility of the two-sided Fourier transform (i.e. $-\infty < k < \infty$ in (11), instead of $0 < k < \infty$) is retained.

(4) The desired flow, at the height z, is obtained by computing the inverse transform according to (AI.2).

The use of a finite Fourier series implies that the topography and the flow will repeat periodically in

both horizontal directions, outside of the computed domain. To avoid the influence from these periodic recurrences of the mountain, we must choose a domain large enough so the unwanted disturbances have decayed to small amplitude near the mountain of interest. At the same time we must choose a sampling interval (ΔX and ΔY) small enough to fully resolve the mountain and the flow. The array size $N_1 = N_2 = 128$ was used for most of the present computations, although occasionally larger arrays were required.

11. Appendix II—Far-field asymptotics

Equation (20) is of the form

$$I = \int_a^b \frac{e^{ig(\psi)}\, d\psi}{(1 - if(\psi))^2}$$

where $f(\psi)$ is generally large but is zero at the points ψ_i. Near to ψ_i, $f(\psi) = f'\alpha$, $g(\psi) = g(\psi_i) + g'|_{\psi_i}\alpha$ where $\alpha \equiv \psi - \psi_i$. Since the contributions to I come primarily from points near to ψ_i we can approximate $I \approx \sum_i I_i$ where

$$I_i = e^{ig(\psi_i)} \int_{-\infty}^{\infty} \frac{e^{ig'\alpha}\, d\alpha}{(1 - if'\alpha)^2}$$

This integral can be evaluated by contour integration, in terms of the residue of the double pole which lies at $\alpha = -i/f'$. If g' is positive/negative the contour of integration must be completed in the upper/lower half of the complex plane. Thus, if g' and f' have the same sign, the contour encloses no singularities and $I_i = 0$. If g' and f' have opposite signs, the contour includes the double pole and

$$I_i = \frac{2\pi\, e^{ig(\psi_i)} |g'| e^{g'/f'}}{(f')^2}$$

For the case at hand, $a = 0$, $b = 2\pi$

$$g(\psi) = \frac{Nz}{U \cos\psi}$$

so

$$g'(\psi) = \frac{Nz}{U} \frac{\sin\psi}{\cos^2\psi}$$

and

$$f'(\psi) = \frac{r}{a} \cos(\psi - \theta)$$

so

$$f'(\psi) = -\frac{r}{a} \sin(\psi - \theta)$$

The function $f(\psi)$ has two zeroes in a 2π interval at

$$\psi_i = \pm\frac{\pi}{2} + \theta$$

so

$$f'(\psi_i) = \mp\frac{r}{a}$$

and

$$g(\psi_i) = \mp\frac{Nz}{U} \frac{1}{\sin\theta}$$

$$g'(\psi_i) = \pm\frac{Nz}{U} \frac{\cos\theta}{\sin^2\theta}$$

Combining these gives

$$\eta(r, \theta, z) = \frac{ha^2}{r^2} \exp\left(-\frac{Nz}{U}\frac{a}{r}\frac{\cos\theta}{\sin^2\theta}\right) \times \left(\frac{Nz}{U}\frac{\cos\theta}{\sin^2\theta}\right) \cdot \left(\exp\left(-i\frac{Nz}{U\sin\theta}\right) + \exp\left(i\frac{Nz}{U\sin\theta}\right)\right)$$

which reduces to (21) in the text.

12. Appendix III—The integration to obtain the surface pressure field

Starting with (36) in the form

$$p'(x, y, 0) = g\frac{d\bar{\rho}}{dz}\frac{U}{N} hI$$

where

$$I = \frac{1}{2\pi}\int_0^{2\pi} \frac{\cos\psi\, d\psi}{i\left(1 - i\frac{r}{a}\cos(\psi - \theta)\right)^2}$$

we introduce a change of variable

$z \equiv e^{i\psi}$ and $z_d \equiv e^{i\theta}$

so that

$$\cos\psi = \frac{1}{2}(z + 1/z)$$

$$\cos\theta = \frac{1}{2}(z_d + 1/z_d)$$

and

$$\cos(\psi - \theta) = \frac{1}{2}\left(\frac{z}{z_d} + \frac{z_d}{z}\right)$$

We now can rewrite I as an integral around a unit circle in the complex plane

$$I = \frac{1}{2\pi}\left(\frac{a}{r}\right)^2 2z_d^2 \oint_{|z|=1} \frac{z^2 + 1\, dz}{(z - z_1)^2 (z - z_2)^2}$$

where z_1 and z_2 are the two double roots of the expression

$$\left(z^2 + 2i\frac{a}{r} z_d z + z_d^2\right)^2$$

so that

$$z_1, z_2 = -iz_d\left(\frac{a}{r} \mp \sqrt{\frac{a^2}{r^2} + 1}\right)$$

The contour integral can be evaluated by the method of residues, recognizing that only the double pole at z_1 lies inside the unit circle. This gives

$$I = \left(\frac{a}{r}\right)^2 \frac{1}{2} \frac{z_d + z_d^{-1}}{\left(\frac{a^2}{r^2} + 1\right)^{3/2}}$$

which is

$$I = \frac{r}{a} \frac{\cos\theta}{\left(1 + \frac{r^2}{a^2}\right)^{3/2}}$$

from which (37) follows.

The integration to obtain $\eta_z(x, y, 0)$ in the form (47) could in principle be done with a similar change of variable. The integral (46) however does not exist as η_z decays too slowly at ∞, so the expression for η_{zx} must first be obtained using the methods above, and then integrated with respect to x.

13. Appendix IV–The wave field at large z

Starting with (20)

$$\eta(r, \theta, z) = \frac{h}{2\pi} \text{Real} \int_0^{2\pi} \frac{e^{im(\psi)z}\, d\psi}{\left(1 - i\frac{r}{a}\cos(\psi - \theta)\right)^2}$$

with $m(\psi) = N/U \cos\psi$, note that for large z the exponential factor will oscillate rapidly causing cancellation, except near $\psi_i = 0, \pi$ where $\cos\psi$ is slowly varying. Near to the ψ_i, $\cos\psi \approx \pm(1 - \frac{1}{2}\alpha^2)$ and

$$m \approx \pm\frac{N}{U}\left(1 + \frac{1}{2}\alpha^2\right)$$

where $\alpha \equiv \psi - \psi_i$. The integral can then be approximated as

$$\eta = \frac{h}{2\pi}\left[\frac{e^{i(N/U)z}}{\left(1 - i\frac{r}{a}\cos\theta\right)^2}\int_{-\infty}^{\infty} e^{i(Nz/2U)\alpha^2}\, d\psi\right.$$

$$\left. + \frac{e^{-i(N/U)z}}{\left(1 + i\frac{r}{a}\cos\theta\right)^2}\int_{-\infty}^{\infty} e^{-i(Nz/2U)\alpha^2}\, d\psi\right]$$

Noting that $r\cos\theta = x$ and that

$$\int_0^\infty \sin bx^2\, dx = \int_0^\infty \cos bx^2\, dx = \frac{1}{2}\sqrt{\frac{\pi}{2b}}$$

reduces the integral to

$$\eta = \frac{h}{2\pi}\left[\frac{e^{i(N/U)z}}{\left(1 - i\frac{x}{a}\right)^2}(1 + i)\sqrt{\frac{\pi}{2}}\sqrt{\frac{2U}{Nz}}\right.$$

$$\left. + \frac{e^{-i(N/U)z}}{\left(1 + i\frac{x}{a}\right)^2}(1 - i)\sqrt{\frac{\pi}{2}}\sqrt{\frac{2U}{Nz}}\right]$$

After carefully separating the real and imaginary parts, the imaginary parts cancel and eq. (34) in the text is obtained.

REFERENCES

Blumen, W. and McGregor, C. D. 1976. Wave drag by three-dimensional mountain lee-waves in nonplanar shear flow. *Tellus 28*, 287–298.

Booker, J. R. and Bretherton, F. P. 1967. The critical layer for internal gravity waves in a shear flow. *J. Fluid Mech. 27*, 513–539.

Crapper, G. D. 1959. A three-dimensional solution for waves in the lee of mountains. *J. Fluid Mech. 6*, 51–76.

Crapper, G. D. 1962. Waves in the lee of a mountain with elliptical contours. *Phil. Trans. Royal Soc. London (A) 254*, 601–623.

Drazin, P. G. 1961. On the steady flow of a fluid of variable density past an obstacle. *Tellus 13*, 239–251.

Gjevik, B. and Marthinsen, T. 1977. Three-dimensional lee-wave pattern. *Quart. J. R. Met. Soc. 104*, 947–957.

Palm, E. 1958. Two-dimensional and three-dimensional mountain waves. *Geophys. Publ. Oslo 20*, 25 pp.

Riley, J. J., Liu, H.-T. and Geller, E. W. 1975. A numerical and experimental study of stably stratified flow around complex terrain. Flow Research Inc., Washington, Report No. 58.

Sawyer, J. S. 1962. Gravity waves in the atmosphere as a three-dimensional problem. *Quart. J. R. Met. Soc. 88*, 412–425.

Scorer, R. S. 1956. Airflow over an isolated hill. *Quart. J. R. Met. Soc. 82*, 75–81.

Scorer, R. S. and Wilkinson, M. 1956. Waves in the lee of an isolated hill. *Quart. J. R. Met. Soc. 82*, 419–427.

Sheppard, P. A. 1956. Airflow over mountains. *Quart. J. R. Met. Soc. 82*, 528.

Smith, R. B. 1979. The influence of mountains on the atmosphere. *Advances in Geophysics*, Vol. 21. New York: Academic Press.

Wurtele, M. 1957. The three dimensional lee wave. *Beitr. Phys. frei. Atmos. 29*, 242–252.

ЛИНЕЙНАЯ ТЕОРИЯ СТРАТИФИЦИРОВАННОГО ГИДРОСТАТИЧЕСКОГО ТЕЧЕНИЯ ЗА ИЗОЛИРОВАННОЙ ГОРОЙ

С помощью линейной теории изучается стратифицированное гидростатическое течение над изолированной горой гладкой формы. При использовании аналитического и численного фурье-анализа получены решения для различных областей течения. Течение вверху характеризуется вертикально распространяющимися горными волнами. Максимальная амплитуда этих волн имеет место непосредственно над горой, но имеется также значительная волновая энергия, распространяющаяся по потоку вдоль парабол $y^2 = Nzax/U$. Вблизи земли приходящие линии тока расщепляются, чтобы избежать препятствия, и это боковое отклонение прослеживается вниз по течению. Горизонтальная дивергенция, связанная с этим боковым отклонением, балансируется опусканием потенциально теплового воздуха сверху. Обсуждается связь линейной теории с трехмерными моделями. Также обсуждаются негеострофические эффекты и предельный случай двумерного бесконечного гребня.